European Journal of Mechanics A/Solids 29 (2010) 826–836

Contents lists available at ScienceDirect

European Journal of Mechanics A/Solids

journal homepage: www.elsevier.com/locate/ejmsol

An efficient procedure to find shape functions and stiffness matrices of nonprismatic Euler–Bernoulli and Timoshenko beam elements

A. Shooshtari [a,*], R. Khajavi [b]

[a] Department of Civil Engineering & Earthquake Research Center, Ferdowsi University of Mashhad, Mashhad, Iran
[b] Department of Civil Engineering, Ferdowsi University of Mashhad, Mashhad, Iran

ARTICLE INFO

Article history:
Received 1 May 2009
Accepted 16 April 2010
Available online 29 April 2010

Keywords:
Euler–Bernoulli formulation
Nonprismatic beam element
Timoshenko formulation

ABSTRACT

Nonprismatic beam modeling is an important issue in structural engineering, not only for versatile applicability the tapered beams do have in engineering structures, but also for their unique potential to simulate different kinds of material or geometrical variations such as crack appearing or spreading of plasticity along the beam. In this paper, a new procedure is proposed to find the exact shape functions and stiffness matrices of nonprismatic beam elements for the Euler–Bernoulli and Timoshenko formulations. The variations dealt with here include both tapering and abrupt jumps in section parameters along the beam element. The proposed procedure has found a simple structure, due to two special approaches: The separation of rigid body motions, which do not store strain energy, from other strain states, which store strain energy, and finding strain interpolating functions rather than the shape functions which suffer complex representation. Strain interpolating functions involve low-order polynomials and can suitably track the variations along the beam element. The proposed procedure is implemented to model nonprismatic Euler–Bernoulli and Timoshenko beam elements, and is verified by different numerical examples.

1. Introduction

Nonprismatic beams have been used in various structures including buildings and bridges since the first decades of the previous century, with an increasing application as the structural engineering techniques were improving. With the beams being tapered, the architects would be able to create and implement novel aesthetic architectural designations, as well as the structural engineers who could seek for optimum low weight - high strength systems through a redistribution of materials along the structural members.

Along with the new improvements in the structural engineering, much interest and attempt was drawn toward finding better formulations to model nonprismatic beam elements. This was not only a consequence of versatile applications the nonprismatic beams found in different engineering structures; but the researches have now recognized that these beams may competently be applied for modeling and simulating some structural phenomena or cases as inelastic behaviors, crack appearance, and different material adoption.

Much research has yet been focused on the issue of nonprismatic beams, all of which may be categorized in the two general branches:

1. Accurate, simple and applicable modeling of nonprismatic beams, and providing suitable differential equations to consider various effects for different analysis types, and
2. Finding simple and applicable methods to solve these differential equations.

This research paper is dealing with the latter.

The governing differential equations were initially been solved by means of exact classical procedures. With the different approximate numerical methods being invented, much research focused on finding solutions for the governing equations based on numerical approaches. Among different methods proposed, finite element method drew much interest, while few attempts considered other approximate techniques such as boundary element method (Al-Gahtani and Khan, 1998).

At the first steps to implement FEM for the analysis of nonprismatic beams, several uniform beam elements were used to discretize the nonprismatic member. Obviously, this technique will not give the exact stiffness matrix for a tapered member, as the real member is substituted by an alternative member composed of several discrete uniform beam elements with different attributes.

* Corresponding author. Tel.: +98 511 8815100x603; fax: +98 511 8763301.
E-mail addresses: ahmadshooshtari@yahoo.com, r_yahya_khajavi@yahoo.com (A. Shooshtari).

0997-7538/$ – see front matter © 2010 Elsevier Ltd. All rights reserved.
doi:10.1016/j.euromechsol.2010.04.003

The analysis will then suffer discretization errors, especially for tapering with sharp gradients. Fine discretization is thus inevitable so that the response does not violate the acceptable tolerance. This will increase analysis expense and time consumption.

Much research has examined different methods to retrieve the stiffness matrix for the nonprismatic beam element. These methods involve direct integration of the governing differential equations (Just, 1977; Karabalis and Beskos, 1983; Biondi and Caddemi, 2007), modifying stiffness methods to consider tapering (Portland Cement Association (PCA), 1958; El-Mezaini et al., 1991; Balkaya, 2001), establishing the flexibility matrix and inversing it (Eisenberger, 1985; Vu-Quoc and Léger, 1992; Frieman and Kosmatka, 1992; Frieman and Kosmatka, 1993; Tena-Colunga, 1996), and applying transfer matrices (Luo et al., 2007; Luo et al., 2006). All these methods may suffer the following deficiencies:

1. Some of these methods will recover the stiffness matrix for some special simple cases of tapering such as linear or parabolic depth variation along rectangular or I-shaped beams; while for other cases, they will be frustrated due to complex representation of shape functions and stiffness matrices (Karabalis and Beskos, 1983; Brown, 1984; Banerjee and Williams, 1986).
2. Some of these methods, such as establishing the flexibility matrix and inversing it, will only retrieve the stiffness matrix, and are unable to recover the shape functions, which might be necessary for the analysis procedure based on stiffness formulation (Eisenberger, 1985; Tena-Colunga, 1996).

This research presents a simple general procedure to establish the stiffness matrix and shape functions of the complex nonprismatic beam elements for the two Euler–Bernoulli and Timoshenko beam formulations. The procedure is based on the separation of rigid body motions from strain states and finding interpolating strain fields rather than deflection (and rotation) field (s) of the beam element. It will give the exact stiffness matrix and interpolating functions for the strain fields of the nonprismatic beam element, apart from the error introduced by numerical integration. Based on these functions, the exact shape functions can be retrieved if they are required for the analysis procedure.

2. Formulation of the procedure

In the following formulation, a finite element with linear elastic behavior is considered in the field of $\Omega = \{(x,y,z) \in R^3$ under arbitrary static loading. The finite element has n_e degrees of freedom, n_r rigid body motions, and $n_s = n_e - n_r$ strain states.

The procedure is established based on the stiffness formulation. According to this formulation, degrees of freedom are successively given a unit displacement, while all others are restrained against any movement. The reactions corresponding to the degrees of freedom will then be determined to recover one column of the stiffness matrix of the finite element. As a mathematical point of view, this corresponds to establishing canonical (standard) basis for the vector space of the element displacement. Surely the canonical basis is not the only ensemble of vectors which may be considered for the element displacement space; An infinite number of basis can be selected to span this vector space. The only criterion each basis should qualify is that its vectors be linearly independent.

In the present formulation, canonical basis is not any longer considered to establish the stiffness matrix of the finite element. Rather, basis vectors are selected so that they can be categorized into two partitions, corresponding to the rigid body motions and strain states of the finite element:

$$\boldsymbol{\Phi}_q = \left[\boldsymbol{\phi}_{qr} : 1 \le r \le n_r \middle| \boldsymbol{\phi}_{qs} : n_r + 1 \le s \le n_e\right] = \left[\boldsymbol{\Phi}_{qr} \middle| \boldsymbol{\Phi}_{qs}\right]. \quad (1)$$

$\boldsymbol{\Phi}_q$ is a columnar arrangement of n_e arbitrary linearly independent basis vectors, which will be addressed as *basis matrix* henceforth. The submatrix $\boldsymbol{\Phi}_{qr}$ includes n_r basis vectors $\boldsymbol{\phi}_{qr}$, corresponding to the rigid body motions, while in the submatrix $\boldsymbol{\Phi}_{qs}$, n_s basis vectors $\boldsymbol{\phi}_{qs}$, corresponding to the arbitrary strain states are arranged.

The first step for the present formulation is the selection of basis vectors for the displacement space, so that they can be divided into two partitions according to Eq. (1). An appropriate choice for the basis vectors may help simplify the procedure to find the stiffness matrix and shape functions. This is briefly discussed in Section 5.

When the basis vectors are selected, they will successively be applied to the element. The strain fields for each basis vector will then be obtained. This will be done using the principle of virtual forces. Assuming a compatible situation between the nodal displacements in the basis vector $\boldsymbol{\phi}_{qk}$ and the corresponding strain fields, variations of virtual equilibrated forces and stresses are applied, and the internal and external virtual works are set as equal:

$$\delta \boldsymbol{P}_k^T \boldsymbol{\phi}_{qk} = \int_{\Omega} \delta \boldsymbol{\sigma}_k^T \varepsilon_k \mathrm{d}\Omega \quad (2)$$

Here, ε_k is the strain field appeared in the domain when $\boldsymbol{\phi}_{qk}$ is applied to the finite element. The virtual stress field $\delta\boldsymbol{\sigma}_k$ is in equilibrium with an applied virtual load $\delta\boldsymbol{P}_k$, or in a more general statement, the virtual stress field is such that $\mathrm{div}\delta\boldsymbol{\sigma}_k$ vanishes in the whole domain, and $\delta\boldsymbol{\sigma}_k\boldsymbol{n}$ equilibrates the virtual traction load on the whole boundary, where $\boldsymbol{n}$ denotes outward unit normal vector on the boundary.

The nodal force vector, $\boldsymbol{P}_k$, is composed of the two following parts:

$$\boldsymbol{P}_k = \{\boldsymbol{P}_{dk} | \boldsymbol{P}_{ik}\}^T \quad (3)$$

$\boldsymbol{P}_{dk}$ is an arbitrary part of nodal force vector with a dimension equal to the degree of static determinacy of the finite element. $\boldsymbol{P}_{ik}$ involves the rest of vector entries. $\boldsymbol{P}_k$ and $\boldsymbol{P}_{dk}$ are related to each other according to the following equation:

$$\boldsymbol{P}_k = \boldsymbol{S}\boldsymbol{P}_{dk} \quad (4)$$

$\boldsymbol{S}$ is the transformation matrix for the inclusion of rigid body modes. Based on the static equilibrium equations, the internal stress field can be obtained from the nodal forces $\boldsymbol{P}_{dk}$:

$$\boldsymbol{\sigma}_k = \boldsymbol{b}\boldsymbol{P}_{dk} \quad (5)$$

The constitutive law is described by the following relation:

$$\varepsilon_k = \boldsymbol{C}\boldsymbol{\sigma}_k \quad (6)$$

Eq. (5) and Eq. (6) will give the following equation:

$$\varepsilon_k = \boldsymbol{C}\boldsymbol{b}\boldsymbol{P}_{dk} \quad (7)$$

By substituting Eqs. (5), (6) and (7) in Eq. (2), the following system of equations is obtained:

$$\int_{\Omega} \boldsymbol{b}^T \boldsymbol{C}\boldsymbol{b}\mathrm{d}\Omega \cdot \boldsymbol{P}_{dk} = \boldsymbol{S}^T \boldsymbol{\phi}_{qk} \quad (8)$$

This system of equation represents the flexibility relation at the element level corresponding to the basis vector $\boldsymbol{\phi}_{qk}$, and may be rewritten as below:

$$\boldsymbol{F}\boldsymbol{P}_{dk} = \boldsymbol{S}^T \boldsymbol{\phi}_{qk} \quad (9)$$

Here, $\boldsymbol{F}$ is the flexibility matrix of the finite element. Solving the system of equations will give $\boldsymbol{P}_{dk}$:

$$\boldsymbol{P}_{dk} = \boldsymbol{F}^{-1}\boldsymbol{S}^T \boldsymbol{\phi}_{qk} \quad (10)$$

Replacing $\boldsymbol{P}_{\mathrm{dk}}$ in Eq. (7), the strain fields corresponding to the basis vector $\boldsymbol{\phi}_{\mathrm{qk}}$, ε_{k}, will be obtained. The vector ε_{k} comprises one column of the $\boldsymbol{B}_{\mathrm{q}}$ matrix which relates the strain and displacement fields in the generalized basis, $\boldsymbol{\Phi}_{\mathrm{q}}$:

$$\boldsymbol{B}_{\mathrm{qk}} = \varepsilon_{\mathrm{k}} = \boldsymbol{CbF}^{-1}\boldsymbol{S}^{T}\boldsymbol{\phi}_{\mathrm{qk}} \tag{11}$$

Eq. (11) plays a fundamental role for the proposed procedure.

When the above process is accomplished for all basis vectors, $\boldsymbol{B}_{\mathrm{q}}$ will then be obtained:

$$\boldsymbol{B}_{\mathrm{q}} = \left[\boldsymbol{B}_{\mathrm{qk}} : 1 \le k \le n_{\mathrm{e}}\right] \tag{12}$$

The matrix $\boldsymbol{B}_{\mathrm{q}}$ can be divided as below, according to the partitioning introduced in Eq. (1):

$$\boldsymbol{B}_{\mathrm{q}} = \left[\boldsymbol{B}_{\mathrm{qr}} : 1 \le r \le n_{\mathrm{r}} \middle| \boldsymbol{B}_{\mathrm{qs}} : n_{\mathrm{r}}+1 \le s \le n_{\mathrm{e}}\right] = \left[\boldsymbol{B}_{\mathrm{qr}} \middle| \boldsymbol{B}_{\mathrm{qs}}\right] \tag{13}$$

As no strain will be recovered when basis vectors corresponding to the rigid body motions are applied to the finite element, The submatrix $\boldsymbol{B}_{\mathrm{qr}}$ is zero. $\boldsymbol{B}_{\mathrm{q}}$ can then be rewritten as following:

$$\boldsymbol{B}_{\mathrm{q}} = \left[\boldsymbol{0}_{n_{\mathrm{r}}} \middle| \boldsymbol{B}_{\mathrm{qs}}\right] \tag{14}$$

Therefore, there is no need to perform the process for the rigid body motions. Using $\boldsymbol{B}_{\mathrm{q}}$, the stiffness matrix in the basis of $\boldsymbol{\Phi}_{\mathrm{q}}$ can easily be obtained:

$$\boldsymbol{K}_{\mathrm{q}} = \int_{\Omega} \boldsymbol{B}_{\mathrm{q}}^{T}\boldsymbol{C}^{-1}\boldsymbol{B}_{\mathrm{q}}\mathrm{d}V \tag{15}$$

This stiffness matrix will have the following representation:

$$\mathbf{K}_{\mathrm{q}} = \begin{bmatrix} \boldsymbol{0}_{n_{\mathrm{r}}\times n_{\mathrm{r}}} & \boldsymbol{0}_{n_{\mathrm{r}}\times n_{\mathrm{s}}} \\ \boldsymbol{0}_{n_{\mathrm{s}}\times n_{\mathrm{r}}} & \mathbf{K}_{\mathrm{qss}} \end{bmatrix}_{n_{\mathrm{e}}\times n_{\mathrm{e}}} \tag{16}$$

The submatrix $\boldsymbol{K}_{\mathrm{qss}}$ is of dimension $n_{\mathrm{s}} \times n_{\mathrm{s}}$, and has a nonzero constant representation when linear elastic behavior is only concerned (Khajavi, 2004).

The matrix of shape functions in the basis of $\boldsymbol{\Phi}_{\mathrm{q}}$, $\boldsymbol{N}_{\mathrm{q}}$, can be obtained from $\boldsymbol{B}_{\mathrm{q}}$, based on the compatibility relations between displacement and strain fields, by some integration process. When there is no need to the shape functions during the analysis procedure, e.g. if dynamics or distributed loads are not considered, this step can be skipped.

When $\boldsymbol{B}_{\mathrm{q}}$, $\boldsymbol{N}_{\mathrm{q}}$, and $\boldsymbol{K}_{\mathrm{q}}$ are obtained for the basis $\boldsymbol{\Phi}_{\mathrm{q}}$, their counterparts in the canonical basis $\boldsymbol{B}$, $\boldsymbol{N}$, and $\boldsymbol{K}$ can easily be obtained through the following transformations:

$$\boldsymbol{B} = \boldsymbol{B}_{\mathrm{q}}.\boldsymbol{\Phi}_{\mathrm{q}}^{-1} \tag{17}$$

$$\boldsymbol{N} = \boldsymbol{N}_{\mathrm{q}}.\boldsymbol{\Phi}_{\mathrm{q}}^{-1} \tag{18}$$

$$\boldsymbol{K} = \boldsymbol{\Phi}_{\mathrm{q}}^{-T}.\boldsymbol{\Phi}_{\mathrm{q}}^{-1} \tag{19}$$

When these matrices are obtained, they can be employed in the well-known linear elastic analysis procedures.

3. Procedure for straight nonprismatic Euler–Bernoulli beam element

In this section, the elastic linear beam element with linear geometrical behavior is considered on the domain $\Omega = \{(x,y,z) \in R^3 | x \in [0,L] \equiv \Omega_{\mathrm{L}} \subset R,\ (y,z) \in \Omega_{\mathrm{A}} \subset R^2\}$ and under arbitrary static loading. In the present formulation, Ω_{A} may not be constant along $\Omega_{\mathrm{L}} \equiv [0,L]$, and might vary arbitrarily unless formulation assumptions are disturbed. It is assumed that the neutral axis is straight, so that arching action, as described by El-Mezaini et al. (1991), may not develop along element. The independent displacement field for this formulation is deflection $w(x)$, from which other fields can be derived based on compatibility relations and constitutive law. The beam element has two nodes at the two ends, with two degrees of freedom of deflection and rotation for each node. The well-known governing differential equation for the two-dimensional Euler–Bernoulli beam is as below:

$$M(x) = EI_z(x)\partial_{xx}w(x) \tag{20}$$

Here, $\partial_{xx}()$ represents second differentiation with respect to x. M, E, and I_z are internal moment, elastic modulus, and second moment of inertia around z respectively.

Based on the above assumptions, the basis vector $\boldsymbol{\phi}_{\mathrm{qk}}$ and the nodal force vector $\boldsymbol{P}_{\mathrm{k}}$ will have the following representations:

$$\boldsymbol{\phi}_{\mathrm{qk}} = \left\{ w_{0\mathrm{k}} = w_{\mathrm{k}}(0) \quad \theta_{0\mathrm{k}} = \theta_{\mathrm{k}}(0) \quad w_{L\mathrm{k}} = w_{\mathrm{k}}(L) \quad \theta_{L\mathrm{k}} = \theta_{\mathrm{k}}(L) \right\}^{T} \tag{21}$$

$$\boldsymbol{P}_{\mathrm{k}} = \left\{ V_{0\mathrm{k}} = V_{\mathrm{k}}(0) \quad M_{0\mathrm{k}} = M_{\mathrm{k}}(0) \quad V_{L\mathrm{k}} = V_{\mathrm{k}}(L) \quad M_{L\mathrm{k}} = M_{\mathrm{k}}(L) \right\}^{T} \tag{22}$$

w, θ, V and M denote deflection, rotation, shear force and moment, respectively. Subscripts 0 and L represent the beginning and end nodes of the nonprismatic beam element respectively, and k is an index for the number of strain state.

In the Euler–Bernoulli formulation, the fields $\boldsymbol{\sigma}_{\mathrm{k}}$ and ε_{k} respectively represent internal moment and curvature along the beam element:

$$\boldsymbol{\sigma}_k \equiv M_k(x) \tag{23}$$

$$\varepsilon_{\mathrm{k}} \equiv \kappa_{\mathrm{k}}(x) \tag{24}$$

Choosing $\boldsymbol{P}_{\mathrm{dk}}$ as the nodal moments at the two ends of the element, the static matrix $\boldsymbol{S}$ is obtained as below (Vu-Quoc and Léger, 1992):

$$\boldsymbol{S}^{T} = \begin{bmatrix} \frac{1}{L} & -1 & -\frac{1}{L} & 0 \\ -\frac{1}{L} & 0 & \frac{1}{L} & 1 \end{bmatrix} \tag{25}$$

When $\boldsymbol{\phi}_{\mathrm{qk}}$ is applied to the element, the resulted moment field is related to $\boldsymbol{P}_{\mathrm{dk}}$ by the following linear interpolation:

$$M_{\mathrm{k}}(x) = \mathbf{b}\mathbf{P}_{dk} = \begin{bmatrix} 1-\frac{x}{L} & \frac{x}{L} \end{bmatrix} \begin{Bmatrix} M_{0k} \\ M_{Lk} \end{Bmatrix} \tag{26}$$

In the Euler–Bernoulli formulation for the nonprismatic beam element, sectional flexibility $\boldsymbol{C}$, which relates the moment and curvature fields, is simply defined as:

$$\boldsymbol{C} = f_{\mathrm{s}}(x) = \frac{1}{EI(x)} \tag{27}$$

With the known matrices $\boldsymbol{C}$ and $\boldsymbol{b}$, the element flexibility matrix $\boldsymbol{F}$ can be obtained. The matrices $\boldsymbol{b}$, $\boldsymbol{C}$, and $\boldsymbol{F}$ are independent of the selected basis, and are computed once during the procedure. By the use of Eq. (11) for all basis vectors corresponding to the strain states, $\boldsymbol{B}_{\mathrm{q}}$ is obtained. The stiffness matrix in the basis $\boldsymbol{\Phi}_{\mathrm{q}}$ can then be established through Eq. (15). Shape functions can be derived by the following equation:

$$N_{\mathrm{qk}}(x) = \int_0^x \left(\int_0^s B_{\mathrm{qk}}(u)\mathrm{d}u + \theta_{0\mathrm{k}} \right) \mathrm{d}s + w_{0\mathrm{k}} \tag{28}$$

Here, u and s are integrating variables. When $\boldsymbol{N}_{\mathrm{q}}$, $\boldsymbol{B}_{\mathrm{q}}$, and $\boldsymbol{K}_{\mathrm{q}}$ are obtained, $\boldsymbol{N}$, $\boldsymbol{B}$, and $\boldsymbol{K}$ are attained by the application of Eqs. (17)–(19).

It is notable that axial and torsional stiffness calculations may also be included and treated in a same way. The virtual work expression should then involve terms to account for axial and torsional strain energy as well. Bending, axial and torsional behavior are mostly regarded as uncoupled (Eisenberger, 1991); however, coupling may simply be introduced in the constitutive relation (Somashekar, 1983). For the proposed formulation, coupling might be included in the off-diagonal entries of sectional flexibility matrix, $\boldsymbol{C}$. It is noticed that warping torsion is frequently excluded from formulation, as it is a secondary effect in beams of building frames (Takabatake, 1990).

4. Procedure for straight nonprismatic Timoshenko beam element

The assumptions made here are the same as the previous section, except that in the Timoshenko beam formulation, deflection and rotation fields are defined independent of each other. The governing equations for the Timoshenko beam are as below:

$$M(x) = EI_z(x)\kappa(x) \tag{29}$$

$$V(x) = GA_s(x)\gamma(x) \tag{30}$$

$$\kappa(x) = \partial_x\theta(x) \tag{31}$$

$$\gamma(x) = \theta(x) - \partial_x w(x) \tag{32}$$

Here, $\partial_x()$ represents first differentiation with respect to x. V, G, and γ are the internal shear, shear modulus, and shear strain respectively. A_s is the shear area which equals the section area multiplied by the shape factor for shear, k_s, and might not be constant along the element as is the case for I_z:

$$A_s(x) = k_s A(x) \tag{33}$$

In the Timoshenko formulation, $\boldsymbol{\sigma}_k$ represents the vector of internal moment and shear, and $\boldsymbol{\varepsilon}_k$ denotes the vector of curvature and shear strain along the beam element:

$$\boldsymbol{\sigma}_k \equiv \begin{Bmatrix} M_k(x) \\ V_k(x) \end{Bmatrix} \tag{34}$$

$$\boldsymbol{\varepsilon}_k \equiv \begin{Bmatrix} \kappa_k(x) \\ \gamma_k(x) \end{Bmatrix} \tag{35}$$

When $\boldsymbol{\phi}_{qk}$ is applied to the element, the resulted moment and shear fields are related to $\boldsymbol{P}_{dk}$ by the following interpolation:

$$\begin{Bmatrix} M_k(x) \\ V_k(x) \end{Bmatrix} = \boldsymbol{b}\boldsymbol{P}_{dk} = \begin{bmatrix} 1-\frac{x}{L} & \frac{x}{L} \\ -\frac{1}{L} & \frac{1}{L} \end{bmatrix} \begin{Bmatrix} M_{0k} \\ M_{Lk} \end{Bmatrix} \tag{36}$$

In the Timoshenko formulation for the nonprismatic beam element, sectional flexibility $\boldsymbol{C}$ is defined as:

$$\boldsymbol{C} = \begin{bmatrix} f_{s11}(x) & f_{s12}(x) \\ f_{s21}(x) & f_{s22}(x) \end{bmatrix} \tag{37}$$

Sectional flexibility matrix is usually assumed as being diagonal for most Timoshenko formulations; however, it is verified that it does have a non-diagonal representation when nonprismatic beam modeling is concerned (Vu-Quoc and Léger, 1992).

Similar to the procedure performed for the Euler–Bernoulli formulation, the element flexibility matrix $\boldsymbol{F}$ is obtained from the matrices $\boldsymbol{b}$ and $\boldsymbol{C}$, and $\boldsymbol{B}_{qk}$ will then be found using Eq. (11). This matrix has the following representation:

$$\boldsymbol{B}_{qk} = \begin{bmatrix} B^{\kappa}_{qk} \\ B^{\gamma}_{qk} \end{bmatrix} \tag{38}$$

Here, $B_{qk}{}^{\kappa}$ and $B_{qk}{}^{\gamma}$ respectively represent the interpolating functions for the curvature and shear strain fields corresponding to $\boldsymbol{\phi}_{qk}$. Finding all these functions for the basis vectors representing strain states, $\boldsymbol{B}_q$ is obtained:

$$\boldsymbol{B}_q = [\boldsymbol{0}_{2\times 2}|\boldsymbol{B}_{qs}] = \left[\begin{array}{c} \boldsymbol{0}_{1\times 2}|\boldsymbol{B}^{\kappa}_{qs} \\ \hline \boldsymbol{0}_{1\times 2}|\boldsymbol{B}^{\gamma}_{qs} \end{array}\right] = \left[\begin{array}{c} \boldsymbol{B}^{\kappa}_{q} \\ \hline \boldsymbol{B}^{\gamma}_{q} \end{array}\right] \tag{39}$$

The stiffness matrix in the basis $\boldsymbol{\Phi}_q$ is derived by the application of Eq. (15). Based on the compatibility relation in Eqs. (31) and (32), the shape functions can be obtained by the following equation:

$$N_{qk}(x) = \int_0^x \left(\int_0^s B^{\kappa}_{qk}(u)\mathrm{d}u + \theta_{0k} \right) \mathrm{d}s - \int_0^x B^{\gamma}_{qk}(u)\mathrm{d}u + w_{0k} \tag{40}$$

With $\boldsymbol{N}_q$, $\boldsymbol{B}_q$, and $\boldsymbol{K}_q$ being known, $\boldsymbol{N}$, $\boldsymbol{B}$, and $\boldsymbol{K}$ will be found by the transformations introduced in Eqs. (17)–(19).

5. Basis selection

Basis vectors representing the strain states can arbitrarily be selected. The only requirement is that they must be linearly independent to be able to span the vector space. Some bases might be preferred to the others, as they will offer simpler representations for the stiffness matrix and shape functions. However, when the stiffness matrix for the element is determined, it has to be transformed to the conventional canonical basis to become ready for the superposition step. Clearly, the canonical basis is the only suitable basis for implementing inter-element compatibility requirements, since it offers nodal displacements and rotations as its vector coefficients.

As mentioned in Section 2, it is strongly recommended to include rigid body motions in the selected basis. This will significantly simplify the procedure to find the stiffness matrix and shape functions, and will reduce computational effort as well. The reason refers to the fact that the element does not store strain energy under rigid body movements. The stiffness matrix is also decoupled for the rigid body motions and deformation states, as implied by Eq. (16). However, this is not the case when geometric stiffness matrix is concerened (Yang and Chiou, 1987).

Basis vectors for representing deformations may arbitrarily be selected according to the analysis requirements. It is noticeable that some bases offer physical implications, and may efficiently be employed for desirable inference. A well-known basis is the one which introduces those basis vectors representing the deformation states the same as the canonical basis vectors corresponding to the rotational degrees of freedom for the beam element:

$$\boldsymbol{\Phi}_q = [\boldsymbol{\Phi}_{qr}|\boldsymbol{\Phi}_{qs}] = \left[\begin{array}{cc|cc} 1 & -L/2 & 0 & 0 \\ 0 & 1 & 1 & 0 \\ 1 & L/2 & 0 & 0 \\ 0 & 1 & 0 & 1 \end{array}\right] \tag{41}$$

This basis is suitable for most applications, and is the one implicitly considered for the flexibility-based formulations.

Another useful basis might be adopted from the strain gradient notation (Dow, 1999), with the following matrix representation:

$$\boldsymbol{\Phi}_q = [\boldsymbol{\Phi}_{qr}|\boldsymbol{\Phi}_{qs}] = \left[\begin{array}{cc|cc} 1 & -L/2 & L^2/8 & -L^3/48 \\ 0 & 1 & -L/2 & L^2/8 \\ 1 & L/2 & L^2/8 & L^3/48 \\ 0 & 1 & -L/2 & L^2/8 \end{array}\right] \tag{42}$$

This basis might be valuable as it provides well-defined strain states. The basis vectors for deformation states represent constant and linear curvature. They can thus be efficiently applied when different effects, such as shear deformations, are investigated for single and double-curvature modes (Vu-Quoc and Léger, 1992). It also offers diagonal stiffness matrix for symmetrical nonprismatic beam elements. The basis in Eq. (42) may also be introduced by Legendre polynomials (Felippa, 2001).

6. Approximate vibration and stability analysis procedures

The formulation introduced in Section 2, may easily be extended to the stability and vibration analysis procedures. It presents the geometric stiffness matrix and the mass matrix which might be used to determine the natural frequencies and buckling loads for plane frame structures, respectively. For the case of simplicity and as the vibration and stability analysis procedures are not the major concern in this research, the formulation is implemented for Euler–Bernoulli theory, and shear and torsion deformations are neglected.

6.1. Vibration analysis

While many authors have employed analytical approaches like Rayleigh–Ritz method to find closed-form solutions for natural frequencies of non-uniform beams (e.g.: Wang, 1967; Auciello and Ercolano, 2004), some others have examined numerical procedures like finite difference (Rissoné and Williams, 1965) and finite element methods.

Lindberg (1963), Gallagher and Lee (1970), To (1981), and Eisenberger and Reich (1989) employed the well-known cubic polynomials to construct the consistent mass matrix for tapered beams. Thomas and Dokumaci (1973) and To (1979) applied higher order polynomials for the vibration analysis. Rutledge and Beskos (1981) and Karabalis and Beskos (1983), though were successful to obtain exact closed-form representations for the stiffness matrix, they failed to do the same for the consistent mass matrix. They alternatively derived the mass matrix from cubic polynomials to perform vibration analysis. The same problem arises when flexibility-based methods are involved.

In this research, mass matrix in the basis of $\boldsymbol{\Phi}_q$ is obtained by the following equation:

$$\boldsymbol{M}_q = \int_0^L \rho \boldsymbol{N}_q^T(x)\boldsymbol{N}_q(x)A(x)\mathrm{d}x \tag{43}$$

where ρ is density, and $A(x)$ is the cross section area. $\boldsymbol{N}_q(x)$ incorporates all functions $N_{qk}(x)$ for strain states k, introduced in Eq. (28). When $\boldsymbol{M}_q$ is obtained, it is transformed to the canonical basis. The mass matrices for the non-uniform elements are then assembled to give the global mass matrix of the structure, $\boldsymbol{M}_s$.

To perform vibration analysis by finite element method, the following eigenproblem is solved:

$$\left(\boldsymbol{K}_s + \omega_i^2 \boldsymbol{M}_s\right)\boldsymbol{D}_{si} = \boldsymbol{0} \tag{44}$$

where ω_i is the natural frequency for mode i, with the mode shape described by eigenvector $\boldsymbol{D}_{si}$, and $\boldsymbol{K}_s$ is the global stiffness matrix. The solution will give the natural frequencies for the specified number of modes.

It is notable that the mass matrix introduced by Eq. (43) is not dynamically consistent, since the shape functions $\boldsymbol{N}_q$ are derived from static, rather than dynamic, equilibrium equations, as described by Eq. (2). This will give rise to some errors in deriving natural frequencies, especially for higher vibrational modes (Cleghorn and Tabarrok, 1992). The vibration analysis will thus be approximate.

6.2. Stability analysis

Many previous studies examined the elastic stability of nonprismatic columns. cubic polynomial shape functions (Kruchoski and Leonard, 1981;Bradford and Cuk, 1988), Bessel functions (Gere and Carter, 1962; Banerjee and Williams, 1986; Saucha and Antunac-Majcen, 2002), Chebyshev polynomials (Li and Li, 2004), power series(Dube and Dumir, 1996; Al-Sadder, 2004) and direct integration of the differential equations (Karabalis and Beskos, 1983; Bazeos and Karabalis, 2006) are generally employed to determine the geometric stiffness matrix for the stability analysis.

In the proposed procedure, approximate geometric stiffness matrix is obtained by the following equation:

$$\boldsymbol{K}_{Gq} = P\int_0^L \boldsymbol{Q}_q^T(x)\boldsymbol{Q}_q(x)\mathrm{d}x \tag{45}$$

where P denotes the axial force, and $\boldsymbol{Q}_q(x)$ is determined from $\boldsymbol{B}_q(x)$, by the following equation for each strain state k:

$$Q_{qk}(x) = \int_0^x B_{qk}(s)\mathrm{d}s + \theta_{0k} \tag{46}$$

$\boldsymbol{B}_{qk}$ is previously introduced in Eq. (11), and θ_{0k} is adopted from Eq. (21). Once $\boldsymbol{K}_{Gq}$ is obtained, Eq. (19) is applied to give the geometric stiffness matrix in the canonical basis. The elastic and geometric stiffness matrices for all members of the structure are then assembled and employed to determine the critical load through the following eigenproblem:

$$(\boldsymbol{K}_s + P_{cr}\boldsymbol{K}_{Gs})\boldsymbol{D}_s = \boldsymbol{0} \tag{47}$$

$\boldsymbol{K}_s$ and $\boldsymbol{K}_{Gs}$ are the global elastic and geometric stiffness matrices of the structure, respectively. P_{cr} is the critical load, with the buckling mode known by the eigenvector $\boldsymbol{D}_s$.

A keypoint is that the previous formulations for the stability analysis try to construct the geometric stiffness matrix through derivatives of shape functions; however, the proposed procedure determines this matrix by performing integration. It can then be easily implemented in finite element codes, as numerical integration procedures are sufficiently straightforward. As was the case for the mass matrix, the geometric stiffness matrix $\boldsymbol{K}_{Gq}$ introduced in Eq. (45) may not be considered exact, since the shape functions $\boldsymbol{N}_q$ are not obtained from nonlinear static equilibrium equations. The geometric stiffness mass matrix will then yield an approximate value for the critical load (Karabalis and Beskos, 1983).

7. Numerical verification

7.1. Nonprismatic cantilever Euler–Bernoulli beam

7.1.1. Static analysis

The nonprismatic beam with three separate segments, shown in Fig. 1, is considered, and clamped at the left end. This example is notable as it will illustrate the efficiency of the procedure to deal with both kinds of discrete and smooth discontinuities simultaneously. The first half of the beam is tapered smoothly, with the depth of the rectangular section varying linearly from $2h$ to h. At the midpoint of the second half, section depth drops abruptly from h to $h/2$. Euler–Bernoulli assumptions are considered for the beam formulation.

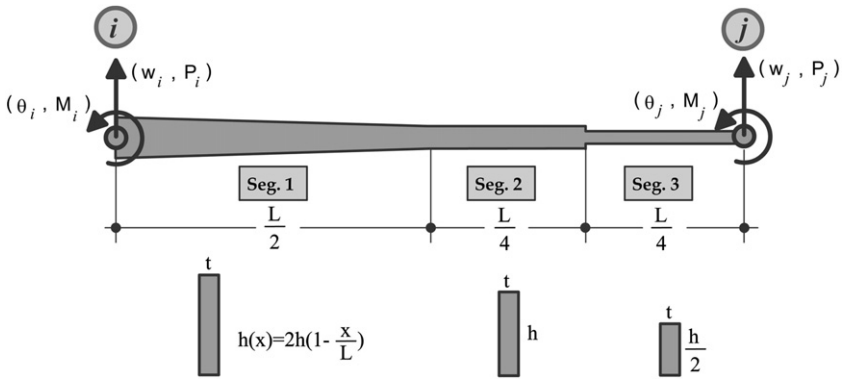

Fig. 1. Sample nonprismatic cantilever beam.

The sample beam with the length $L = 8$ m , depth $h = 0.4$ m , thickness $t = 0.1$ m , density $\rho = 7850$ kg/m^3 , and elastic modulus $E = 210$ GPa , under two types of concentrated load $P_j = 50$ kN at the free tip, and uniform distributed load $p = 10$ kN/m, is analyzed by the three following methods:

1. Modeling the cantilever beam as one nonprismatic Euler–Bernoulli beam element, with the stiffness matrix and shape functions obtained by the procedure proposed in Section 3.
2. Modeling the cantilever beam by three Euler–Bernoulli beam elements, corresponding to the three separate sections. The exact stiffness matrix and shape functions for the tapered element representing segment (1) are derived according to Franciosi and Mecca (1998). The same expressions are obtained if the proposed procedure is applied to this segment.
3. Modeling the cantilever beam by quadrilateral membrane elements with a maximum dimension of 0.1 m. This is a near-optimum finite element mesh, with accuracy better than 2.5% for displacements and rotations. The membrane element is typical with 4 nodes and 12 degrees of freedom, and employs an iso-parametric formulation including translational in-plane stiffness components and a rotational stiffness component in the direction normal to the plane of the element. The nodes at the clamped end are restrained against displacement and rotation.

For Method (1) (proposed method), the stiffness matrix and the interpolating functions are obtained by the application of the basis in Eq. (41). For the analysis of the beam under the concentrated load at the tip, shape functions are not required, and computational effort might then be decreased; however, for the case of distributed loading, shape functions must inevitably be calculated according to Eqs. (28) and (18). As the interpolating functions $\boldsymbol{N}_q$ benefit simpler representation than $\boldsymbol{N}$, integration is recommended to be performed on $\boldsymbol{N}_q$ functions. For this example, exact integrating over $\boldsymbol{N}$, to find the equivalent nodal forces, is very difficult to be performed for the tapered segment, and numerical integration is inevitable. Rather, by performing exact integration over $\boldsymbol{N}_q$, equivalent forces can be obtained in the basis $\boldsymbol{\Phi}_q$, and will then be transformed to the visible degrees of freedom.

The exact shape functions $\boldsymbol{N}$, obtained by the proposed procedure, are shown in Fig. 2, and reported in Appendix A. Obviously, they do not resemble the well-known polynomials usually been used for nonprismatic beam formulations; rather, they are dependent on the pattern the moment of inertia is distributed along the beam element.

The number of degrees of freedom used in the analysis by the proposed method is simply 2, while this is 6 for Method (2). Therefore, the proposed method is preferred as it will decrease the computational effort, especially when a great number of complex nonprismatic members with similar discontinuity pattern are used in the frame structure. As exact stiffness matrices are employed for Method (2), the results by the two methods (1) and (2) are close to each other, as shown in Table 1. It is notable that when static condensation technique is applied to the global stiffness matrix assembled from the three exact beam elements introduced in Method (2), the same stiffness matrix as the proposed one is obtained. If the exact stiffness matrix for the tapered segment is not employed in Method (2), a great number of small uniform elements are required to hold the results in a reasonable tolerance. This will undoubtedly increase the expense of the analysis procedure (Karabalis and Beskos, 1983).

As indicated in Table 1, the displacements and rotations obtained by the proposed method coincide exactly those obtained by Method (2) for the concentrated loading. This shows that the proposed method has offered exact interpolating functions. However, small discrepancies exist between the responses reported by the two methods (1) and (2) for the points along the beam under the distributed uniform loading. These discrepancies are caused due to different values of equivalent nodal forces provided by the two methods. Obviously, when more elements are used to discretize the member, equivalent nodal forces will resemble the real distribution, and the responses for the interior points will be more accurate. It should be mentioned that the discrepancies observed between the responses obtained by Method (3) with the two others are due to the initial assumptions made in the formulations. As implied by Table 1, the two one-dimensional models (1) and (2) overestimate the stiffness of the member, resulting in smaller deflections and rotations. This is relevant to the low-stress areas

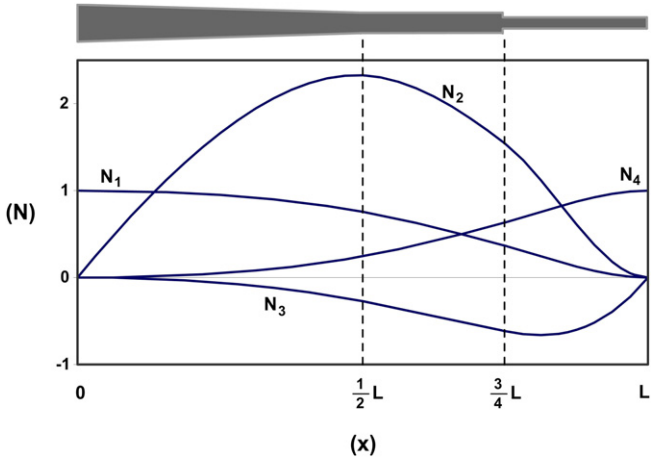

Fig. 2. Exact shape functions for the nonprismatic Euler–Bernoulli beam element with the pattern shown in Fig. 1.

Table 1
Free end displacement obtained by different methods (Euler–Bernoulli beam).

Method	$x = L/2$		$x = 3L/4$		$x = L$	
	Deflection	Rotation	Deflection	Rotation	Deflection	Rotation
	mm	rad	mm	rad	mm	rad
Point loading						
Proposed method	5.51849	0.003571	15.6375	0.006250	37.66135	0.0134
FEM (3 exact EB beam elements)	5.51849	0.003571	15.6375	0.006250	37.66135	0.0134
FEM (membrane elements)	6.26187	0.004838	17.9602	0.007331	41.92648	0.0144
Distributed loading						
Proposed method	2.75351	0.00174	7.537147	0.002873	15.5357	0.0038
FEM (3 exact EB beam elements)	3.506889	0.00198	8.479635	0.002814	15.5357	0.0038
FEM (Membrane elements)	4.08552	0.002631	10.00131	0.003358	18.1858	0.0044

around discontinuous sections, ignored in one-dimensional models as reported by El-Mezaini et al. (1991), and neglecting local taper effects, as quoted by Hodges et al. (2008).

It is notable that the shear and moment distributions along the beam are exactly the same for the two methods (1) and (2), since the structure is statically determinate. It is however noted that the stress distributions, obtained by the first two models, may not be regarded accurate around the discontinuous sections (El-Mezaini et al., 1991).

7.1.2. Vibration analysis

Vibration analysis is performed for the sample nonprismatic cantilever beam by the following three methods:

1. Modeling the cantilever beam as one nonprismatic Euler–Bernoulli beam element, with the stiffness matrix and shape functions obtained by the procedure proposed in Section 3.
2. Modeling the cantilever beam by three Euler–Bernoulli beam elements, corresponding to the three separate sections. The stiffness matrix and shape functions for the tapered element representing segment (1) are obtained according to Tang (1993).
3. Modeling the cantilever beam by uniform Euler–Bernoulli beam elements. Tapered segment of the beam is substituted by 10 uniform beam elements (Stepped beam modeling).

The first and second frequencies of the non-uniform beam are derived, and listed in Table 2. Obviously, the proposed method may not deal with the frequencies beyond the second mode, since the cantilever beam is modeled by only one nonprismatic element with two active degrees of freedom. The consistent mass matrix is derived by the use of shape functions reported in Appendix A.

As shown by Table 2, the values obtained by all three models are close to each other for the first natural frequency; however, a large discrepancy is observed for the second frequency, between the value offered by the proposed method, and those derived by the other two. It seems that the proposed method is unable to predict the second frequency accurately. The reason is due to the fact that the mass matrix introduced by Eq. (43) is statically consistent, as noted in Section 6.1.

Table 2
Critical load factor and natural frequencies obtained by different methods (Euler–Bernoulli beam).

Method	λ_{cr}	f_1 (Hz)	f_2 (Hz)
Proposed method	0.0407	12.2059	70.4928
FEM (3 exact EB beam elements)	0.0389	11.2221	38.3629
FEM (stepped beam modeling)	0.0392	11.6482	38.4468

7.1.3. Stability analysis

The three previous methods, applied for vibration analysis, are used to find the critical load of sample nonprismatic cantilever beam. The results are shown in Table 2. All derivatives and integrals are calculated analytically. $\lambda_{cr} = (P_{cr}L^2)/(\pi^2 EI_0)$ is defined as the critical load factor, where I_0 is the moment of inertia for the section at the clamped end. The values for the three methods are nearly close to each other. The matrix-form eigenproblem dealt with in the proposed method is simply of dimension 2, while it is 6 and 24 for the second and third methods respectively. It is also reminded that no derivatives are needed to be calculated for the proposed procedure.

7.2. Nonprismatic cantilever Timoshenko beam

The previous example with the same features is remodeled and analyzed for the Timoshenko formulation; however, the beam length is set to $L = 2$ m to intensify shear effects. The shear modulus and shape factor are assumed to be $G = 80$ MPa and $k_s = 5/6$ respectively.

The three following methods are applied for the analysis of the sample structure:

1. Modeling the cantilever beam as one nonprismatic Timoshenko beam element, with the stiffness matrix and shape functions obtained by the procedure proposed in Section 4.

Table 3
Free end displacement obtained by different methods (Timoshenko beam).

Method	$x = L/2$		$x = 3L/4$		$x = L$	
	Deflection	Rotation	Deflection	Rotation	Deflection	Rotation
	mm	rad	mm	rad	mm	rad
Point loading						
Proposed method	0.099223	0.000223	0.265812	0.000391	0.62958	0.000837
FEM (3 exact T beam elements)	0.099223	0.000223	0.266708	0.000391	0.62958	0.000837
FEM (membrane elements)	0.093707	0.000239	0.265289	0.00049	0.67367	0.001038
Distributed loading						
Proposed method	0.012066	0.000026	0.03111	0.000043	0.06280	0.000053
FEM (3 exact T beam elements)	0.017449	0.000031	0.03828	0.000044	0.06678	0.000059
FEM (membrane elements)	0.016746	0.000034	0.03843	0.000051	0.070351	0.000066

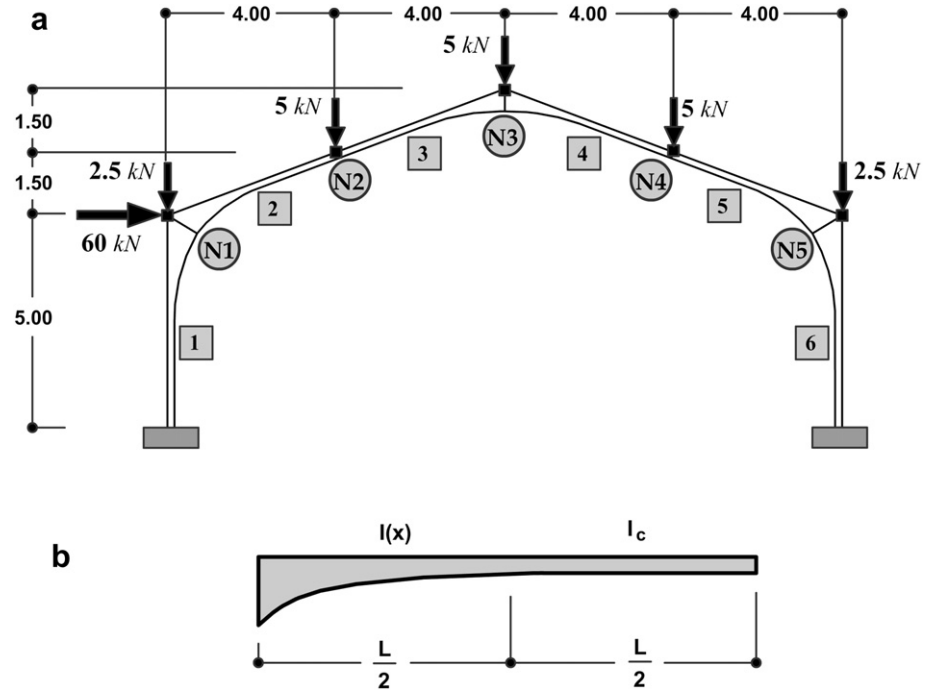

Fig. 3. A gable frame with nonprismatic members. (a) Geometry and loading of the structure (All lengths are given in meters). (b) Discontinuity pattern of the members.

2. Modeling the cantilever beam by three Timoshenko beam elements, corresponding to the three separate segments.
3. Modeling the cantilever beam by quadrilateral membrane elements with a maximum dimension of 0.025 m.

The results for the two types of loading are reported in Table 3. As indicated by Table 3, the responses obtained by the proposed method are duly close to those obtained by the two other methods, while it has applied just one element to model the beam. Table 3 verifies the results pointed out for Table 1. However, a comparison of the two Tables 1 and 3 shows a decrease in the discrepancies observed in Table 3 for the interior nodes in the distributed loading, which is due to the decrease in the length of the beam.

7.3. Gable frame with nonprismatic Euler–Bernoulli members

A gable frame as shown in Fig. 3a is considered. All the members numbered in Fig. 3a share the same discontinuity pattern as shown in Fig. 3b. The nonprismatic member consists of two equal segments. One segment is constant with the moment of inertia $I_c = 78{,}465{,}066\ \text{mm}^4$, and section area $A = 7038\ \text{mm}^2$. The other segment is tapered with the moment of inertia varying as $I = I_c[1 + 3(1 - (2x/L))^2]^3$. Elastic modulus is assumed to be $E = 210$ GPa, and section area is considered constant for the case of simplicity. Any kind of buckling is prevented. It is assumed that the initial curvature of the tapered segment does not violate the Euler–Bernoulli assumption, due to the large centroid axis curvature radius-to-depth ratio. Arching action is also supposed to be negligible (El-Mezaini et al., 1991). The structure is analyzed under the loading shown in Fig. 3a by the two following methods:

1. Modeling each frame member as one nonprismatic Euler–Bernoulli beam element, with the stiffness matrix and shape functions obtained by the procedure proposed in Section 3.
2. Modeling frame members by stepped Euler–Bernoulli beam elements. Tapered segment of each member is substituted by 8 different uniform beam elements with cross sections at mid-length.

As no element loading is applied on the structure, the procedure to find shape functions can be skipped. Following the steps of the proposed procedure, the nonzero section of the bending stiffness matrix in the basis cited in Eq. (41), will be obtained as below:

Table 4
Nodal displacements obtained by different methods (Example 7-3).

Nodes	Method 1 (proposed)			Method 2		
	6 Nonprismatic elements			54 Uniform elements		
	u_X	u_Y	r_Z	u_X	u_Y	r_Z
	mm	mm	rad	mm	mm	rad
N1	30.8493	0.0194	−0.0067	29.8439	0.0059	−0.0068
N2	35.3185	−12.0321	0.0028	34.9545	−13.8315	0.0021
N3	28.3983	6.2884	0.0048	28.4143	3.4261	0.0048
N4	32.7261	18.0104	−0.0007	33.1104	16.1795	−0.0000
N5	25.8938	−0.0279	0.0065	26.9281	−0.0617	0.0065

Table 5
Forces and moments along element 1 obtained by different methods (Example 7-3).

Section no.	z	Method 1 (proposed)			Method 2		
		Axial force	Shear	Moment	Axial force	Shear	Moment
	m	kN	kN	kN m	kN	kN	kN m
10	5.00	5.73	40.31	−99.53	1.76	34.12	−78.66
9	4.69			−86.93			−67.99
8	4.38			−74.34			−57.33
7	4.06			−61.74			−46.67
6	3.75			−49.15			−36.00
5	3.44			−36.55			−25.34
4	3.13			−23.95			−14.68
3	2.81			−11.36			−4.01
2	2.50			1.24			6.65
1	0			102.00			91.96

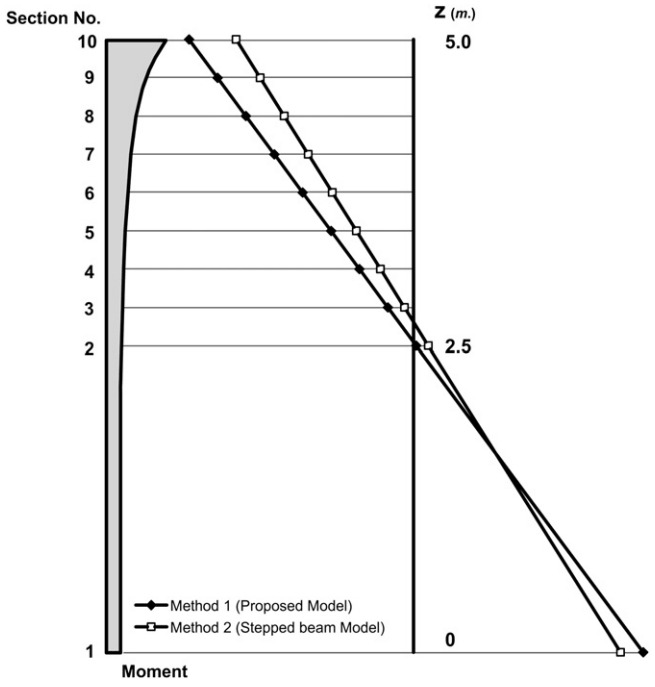

Fig. 4. Moment distribution along element 1 of the gable frame, obtained by the proposed and stepped models.

$$\mathbf{K}_{qss} = \frac{EI_c}{L}\begin{bmatrix} 16.51647 & 6.31396 \\ 6.31396 & 5.55888 \end{bmatrix}$$

This matrix refers to the element with the tapered segment located at the first half of the element. The diagonal entries must be interchanged when the second half of the element is tapered.

Nodal displacements and rotations of the structure, obtained by the two aforesaid methods, are reported in Table 4. Obviously the results share close consistency with each other. However, it is notable that for the proposed method, 6 nonprismatic elements and a total number of 15 degrees of freedom are used, while these numbers are 54 and 159, respectively, for Method (2). As tapered segments of the members are discretized by several uniform elements in Method (2), the results obtained by this method are approximate. However, the proposed method offers exact responses, due to the use of exact stiffness matrix for the nonprismatic element.

In Table 5, axial force, shear and moment values, obtained by the two methods, are reported at some specified sections along element 1 (left column). Fig. 4 illustrates moment distribution along this member. In the absence of distributed loads, moment distribution is simply linear.

8. Conclusion

This research presents a new procedure to obtain the exact stiffness matrix and interpolating functions for the displacement and strain fields of any arbitrary nonprismatic beam element for Euler–Bernoulli and Timoshenko formulations. The proposed procedure is verified as being more efficient in comparison with its rivals:

1. The results obtained by the elements created through the proposed procedure are adequately exact, apart from the error introduced by numerical integration. The procedure provides the exact stiffness matrix and interpolating functions as it is based on the principle of virtual work and considers discontinuities in moment of inertia and shear area to establish the interpolating functions. Specially, the shape functions need to be exact, so that the distributed loads are accurately lumped as equivalent nodal forces. However, the proposed method manipulates structures with nodal loads, better than those with distributed loads. When distributed loads are dealt with, the responses for the interior points along the element are approximate.
2. In the proposed procedure, shape functions are derived from integration performed on the beam element, rather than integrating the differential equation with variable coefficients. The latter is adopted by several authors to introduce general exact expressions for the shape functions, which generally results in complex integrand expressions, e.g. (Karabalis and Beskos, 1983; Eisenberger, 1991). Practically, it is easier to perform integration on the beam element, than to integrate differential equations.
3. The analysis using the finite elements created by the proposed procedure requires less computational effort, since complex discontinuities along each member can be formulated and wrapped into one element. This will decrease the number of degrees of freedom dealt with in the analysis, and dividing a member into several elements to model complex discontinuities will not be any longer needed. Moreover, the interpolating functions in the selected basis might have a simpler representation, and might be manipulated more easily. This will help decrease the analysis expense.
4. The proposed procedure has employed some approaches to reduce computational effort to create finite elements. Separating rigid body motions in the formulation, selecting well-behaved strain states, and searching for strain interpolating functions rather than the shape functions, are the schemes adopted to simplify the process of element creation. The computational effort for the process will notably be reduced if shape functions are not required during the analysis procedure, as is the case when distributed loading does not exist, or dynamic analysis is not concerned. If shape functions are inevitable, they can simply be retrieved from strain interpolating functions as mentioned in the context.
5. The proposed procedure is general, which is able to model a combination of various arbitrary discrete and smooth discontinuities along the finite element. Most methods proposed in the literature, are limited to the analysis of specific kinds of tapering such as linear or parabolic variations. Few authors derived general solutions for arbitrary tapering, and proposed integral expressions which suffer complicated representation. To the authors' knowledge, no previous method is reported which can deal with both discrete and smooth discontinuities along the beam element.
6. The procedure may easily be implemented in finite element codes. The proposed algorithm can automatically develop the element stiffness matrix and shape functions. An interesting feature is that the proposed method needs only integration be computed; this is not the case for other general procedures, where shape functions are developed first, and strain interpolating functions are then obtained through appropriate derivatives. Numerical or automatic differentiation techniques are thus required, in addition to numerical integration schemes, when the stiffness matrix is not to be determined a priori. The proposed procedure, alternatively, develops strain interpolating functions first, and may produce shape functions by integration, if needed. This is more favorable to implement numerical integration rather than differentiation, especially for finite element codes.

7. Due to the generality of the procedure, complicated integrands are likely to arise. Numerical integrations will then be inevitable, which can be computed by any quadrature rule. Gaussian quadrature is widely used for engineering applications, due to its ability to deal with a broad range of functions including polynomials and smooth functions. However, it is not suitable for functions with singularities. Since the proposed procedure deals with elements along which several discontinuities might exist, care must be taken to select an appropriate numerical integration scheme. Stoer and Bulirsch (2002) reported some techniques to deal with different kinds of singularities by means of Gaussian quadrature rules. Many others might be found in the literature, each of which is customized for a special kind of singularity for a particular engineering application. The subject is however beyond the scope of this paper, and must be treated in a further research.

Appendix A

Applying the proposed procedure to create Euler–Bernoulli beam element with discontinuity pattern shown in Fig. 1 and by the use of basis in Eq. (41), the matrices $\boldsymbol{B}_{\mathrm{q}}$, $\boldsymbol{N}_{\mathrm{q}}$, $\boldsymbol{B}$, and $\boldsymbol{N}$ are obtained as below:

For $0 \le x \le L/2$

$$\boldsymbol{B}_{\mathrm{q}}^{\mathrm{T}}(x) = \begin{bmatrix} 0 \\ 0 \\ (1-\frac{x}{L})^{-3}\left(\dfrac{-1.1440}{L}+1.3529\dfrac{x}{L}\right) \\ (1-\frac{x}{L})^{-3}\left(\dfrac{-0.2089}{L}+0.3221\dfrac{x}{L}\right) \end{bmatrix} \qquad (\mathrm{A}-1)$$

$$\boldsymbol{N}_{\mathrm{q}}^{\mathrm{T}}(x) = \begin{bmatrix} 1 \\ x-\frac{L}{2} \\ (1-\frac{x}{L})^{-1}\left(2.3529x+2.2485\frac{x^2}{L}+1.3529\,\mathrm{Ln}(1-\frac{x}{L})(L-x)\right) \\ (1-\frac{x}{L})^{-1}\left(0.3221x-0.2655\frac{x^2}{L}+0.3221\,\mathrm{Ln}(1-\frac{x}{L})(L-x)\right) \end{bmatrix} \qquad (\mathrm{A}-2)$$

$$\boldsymbol{B}^{\mathrm{T}}(x) = \begin{bmatrix} (1-\frac{x}{L})^{-3}\left(\dfrac{-1.3529}{L^2}+1.6751\dfrac{x}{L^3}\right) \\ (1-\frac{x}{L})^{-3}\left(\dfrac{-1.1440}{L}+1.3529\dfrac{x}{L^2}\right) \\ (1-\frac{x}{L})^{-3}\left(\dfrac{1.3529}{L^2}-1.6751\dfrac{x}{L^3}\right) \\ (1-\frac{x}{L})^{-3}\left(\dfrac{-0.2089}{L}+0.3221\dfrac{x}{L}\right) \end{bmatrix} \qquad (\mathrm{A}\text{-}3)$$

$$\boldsymbol{N}^{\mathrm{T}}(x) = \begin{bmatrix} (1-\frac{x}{L})^{-1}\left(1+0.6751\dfrac{x}{L}-1.514\dfrac{x^2}{L^2}+1.6751\,\mathrm{Ln}\left(1-\dfrac{x}{L}\right)\left(1-\dfrac{x}{L}\right)\right) \\ (1-\frac{x}{L})^{-1}\left(2.3529x-2.2485\frac{x^2}{L}+1.3529\,\mathrm{Ln}(1-\frac{x}{L})(L-x)\right) \\ (1-\frac{x}{L})^{-1}\left(-1.6751\dfrac{x}{L}+1.514\dfrac{x^2}{L^2}-1.6751\,\mathrm{Ln}\left(1-\dfrac{x}{L}\right)\left(1-\dfrac{x}{L}\right)\right) \\ (1-\frac{x}{L})^{-1}\left(0.3221x-0.2655\frac{x^2}{L}+0.3221\,\mathrm{Ln}(1-\frac{x}{L})(L-x)\right) \end{bmatrix} \qquad (\mathrm{A}-4)$$

For $L/2 \le x \le 3L/4$

$$\boldsymbol{B}_{\mathrm{q}}^{\mathrm{T}}(x) = \begin{bmatrix} 0 \\ 0 \\ \dfrac{-9.1523}{L}+10.8235\dfrac{x}{L^2} \\ \dfrac{-1.6712}{L}+2.5770\dfrac{x}{L^2} \end{bmatrix} \qquad (\mathrm{A}-5)$$

$$\boldsymbol{N}_{\mathrm{q}}^{\mathrm{T}}(x) = \begin{bmatrix} 1 \\ x-\frac{L}{2} \\ -0.3824L+3.1836x-4.5761\dfrac{x^2}{L}+1.8039\dfrac{x^3}{L^2} \\ -0.0593L+0.3612x-0.8356\dfrac{x^2}{L}+0.4295\dfrac{x^3}{L^2} \end{bmatrix} \qquad (\mathrm{A}-6)$$

$$\boldsymbol{B}^{\mathrm{T}}(x) = \begin{bmatrix} \dfrac{-10.8235}{L^2}+13.4005\dfrac{x}{L^3} \\ \dfrac{-9.1523}{L}+10.8235\dfrac{x}{L^2} \\ \dfrac{10.8235}{L^2}-13.4005\dfrac{x}{L^3} \\ \dfrac{-1.6712}{L}+2.5770\dfrac{x}{L^2} \end{bmatrix} \qquad (\mathrm{A}-7)$$

$$\boldsymbol{N}^{\mathrm{T}}(x) = \begin{bmatrix} 0.5584+2.5448\dfrac{x}{L}-5.4117\dfrac{x^2}{L^2}+2.2334\dfrac{x^3}{L^3} \\ -0.3824L+3.1836x-4.5761\dfrac{x^2}{L}+1.8039\dfrac{x^3}{L^2} \\ 0.4416-2.5448\dfrac{x}{L}+5.4117\dfrac{x^2}{L^2}-2.2334\dfrac{x^3}{L^3} \\ -0.0593L+0.3612x-0.8356\dfrac{x^2}{L}+0.4295\dfrac{x^3}{L^2} \end{bmatrix} \qquad (\mathrm{A}\text{-}8)$$

For $3L/4 \le x \le L$

$$\boldsymbol{B}_{\mathrm{q}}^{\mathrm{T}}(x) = \begin{bmatrix} 0 \\ 0 \\ \dfrac{-73.2183}{L}+86.5877\dfrac{x}{L^2} \\ \dfrac{-13.3694}{L}+20.6161\dfrac{x}{L^2} \end{bmatrix} \qquad (\mathrm{A}-9)$$

$$\boldsymbol{N}_{\mathrm{q}}^{\mathrm{T}}(x) = \begin{bmatrix} 1 \\ x-\frac{L}{2} \\ -7.7466L+29.9244x-36.0609\dfrac{x^2}{L}+14.4314\dfrac{x^3}{L^2} \\ -0.8127L+4.0614x-6.6847\dfrac{x^2}{L}+3.4360\dfrac{x^3}{L^2} \end{bmatrix} \tag{A-10}$$

$$\boldsymbol{B}^{\mathrm{T}}(x) = \begin{bmatrix} \dfrac{-86.5877}{L^2}+107.204\dfrac{x}{L^3} \\ \dfrac{-73.2183}{L}+86.5877\dfrac{x}{L^2} \\ \dfrac{86.5877}{L^2}-107.204\dfrac{x}{L^3} \\ \dfrac{-13.3694}{L}+20.6161\dfrac{x}{L^2} \end{bmatrix} \tag{A-11}$$

$$\boldsymbol{N}^{\mathrm{T}}(x) = \begin{bmatrix} -7.5592+32.9858\dfrac{x}{L}-43.2939\dfrac{x^2}{L^2}+17.8673\dfrac{x^3}{L^3} \\ -7.7466L+29.9244x-36.0609\dfrac{x^2}{L}+14.4314\dfrac{x^3}{L^2} \\ 8.5593-32.9858\dfrac{x}{L}+43.2939\dfrac{x^2}{L^2}-17.8673\dfrac{x^3}{L^3} \\ -0.8127L+4.0614x-6.6847\dfrac{x^2}{L}+3.4360\dfrac{x^3}{L^2} \end{bmatrix} \tag{A-12}$$

References

Al-Gahtani, H.J., Khan, M.S., 1998. Exact analysis of nonprismatic beams. Journal of Engineering Mechanics ASCE 124 (11), 1290–1293.

Al-Sadder, S.Z., 2004. Exact expressions for stability functions of a general non-prismatic beam–column member. Journal of Constructional Steel Research 60, 1561–1584.

Auciello, N.M., Ercolano, A., 2004. A general solution for dynamic response of axially loaded non-uniform Timoshenko beams. International Journal of Solids and Structures 41, 4861–4874.

Balkaya, C., 2001. Behavior and modeling of nonprismatic members having T-sections. Journal of Structural Engineering ASCE 127 (8), 940–946.

Banerjee, J.R., Williams, F.W., 1986. Exact Bernoulli-Euler static stiffness matrix for a range of tapered beam-columns. International Journal for Numerical Methods in Engineering 23, 1615–1628.

Bazeos, N., Karabalis, D.L., 2006. Efficient computation of buckling loads for plane steel frames with tapered members. Engineering Structures 28, 771–775.

Biondi, B., Caddemi, S., 2007. Euler–Bernoulli beams with multiple singularities in the flexural stiffness. European Journal of Mechanics A-Solids 26, 789–809.

Bradford, M.A., Cuk, P.E., 1988. Elastic buckling of tapered monosymmetric I-beams. Journal of Structural Engineering ASCE 114 (5), 977–996.

Brown, C.J., 1984. Approximate stiffness matrix for tapered beams. Journal of Structural Engineering ASCE 110 (12), 3050–3055.

Cleghorn, W.L., Tabarrok, B., 1992. Finite element formulation of a tapered Timoshenko beam for free lateral vibration analysis. Journal of Sound and Vibration 152, 461–470.

Dow, J.O., 1999. A Unified Approach to the Finite Element Method and Error Analysis Procedures. Academic Press.

Dube, G.P., Dumir, P.C., 1996. Tapered thin open section beams on elastic foundation—buckling analysis. Computers and Structures 61 (5), 845–857.

Eisenberger, M., Reich, Y., 1989. Static, vibration and stability analysis of non-uniform beams. Computers and Structures 31, 567–573.

Eisenberger, M., 1985. Explicit stiffness matrices for non-prismatic members. Computers and Structures 20 (4), 715–720.

Eisenberger, M., 1991. Exact solution for general variable cross-section members. Computers and Structures 41 (4), 765–772.

El-Mezaini, N., Balkaya, C., Citipitioglu, E., 1991. Analysis of frames with nonprismatic beam elements. Journal of Structural Engineering ASCE 117 (6), 1573–1592.

Felippa, C.A., 2001. Customizing high performance elements by Fourier methods. Trends in Computational Structural Mechanics. CIMNE, Barcelona, Spain.

Franciosi, C., Mecca, M., 1998. Some finite elements for the static analysis of beams with varying cross section. Computers and Structures 69, 191–196.

Frieman, Z., Kosmatka, J.B., 1992. Exact stiffness matrix of a nonuniform beam—extension, torsion and bending of a Bernoulli-Euler beam. Computers and Structures 42 (5), 671–682.

Frieman, Z., Kosmatka, J.B., 1993. Exact stiffness matrix of a nonuniform beam—bending of a Timoshenko beam. Computers and Structures 49 (3), 545–555.

Gallagher, R.H., Lee, C.H., 1970. Matrix dynamic and instability analysis with non-uniform elements. International Journal for Numerical Methods in Engineering 2, 265–275.

Gere, J.M., Carter, W.O., 1962. Critical buckling loads for tapered columns. Journal of the Structural Division ASCE 88 (1), 1–11.

Hodges, D.H., Ho, J.C., Yu, W., 2008. The effect of taper on section constants for in-plane deformation of an isotropic strip. Journal of Mechanics of Materials and Structures 3 (3), 425–440.

Just, D.J., 1977. Plane frameworks of tapering box and I-section. Journal of the Structural Division ASCE 103 (1), 71–86.

Karabalis, D.L., Beskos, D.E., 1983. Static, dynamic and stability analysis of structures composed of tapered beams. Computers and Structures 16 (6), 731–748.

Khajavi, R., 2004. Partitioning the stiffness matrix and the principal stiffness matrix of the finite element. M.Sc. Dissertation, Ferdowsi University of Mashhad, Iran (in Farsi).

Kruchoski, B.L., Leonard, J.W., 1981. Stability of nonprismatic. Engineering Structures 3, 52–61.

Li, J., Li, G., 2004. Buckling analysis of tapered lattice columns using a generalized finite element. Communications in Numerical Methods in Engineering 20, 479–488.

Lindberg, G.M., 1963. Vibration of non-uniform beams. Aeronautical Quarterly 14, 387–395.

Luo, Y., Wu, F., Xu, X., 2006. Element stiffness matrix and modified coefficients for circular tube with tapered ends. Journal of Constructional Steel Research 62, 856–862.

Luo, Y.Z., Xu, X., Wu, F., 2007. Accurate stiffness matrix for nonprismatic members. Journal of Structural Engineering ASCE 133 (8), 1168–1175.

Portland Cement Association (PCA), 1958. Handbook of frame constants: beam factors and moment coefficients for members of variable section. Skokie, III.

Rissoné, R.F., Williams, J.J., 1965. Vibrations of non-uniform cantilever beams. The Engineer 220, 497–506.

Rutledge, W.D., Beskos, B.E., 1981. Dynamic analysis of linearly tapered beams. Journal of Sound and Vibration 79 (3), 457–462.

Saucha, J., Antunac-Majcen, M., 2002. General approach to the determination of critical buckling loads for tapered columns. Transactions of Famena 26 (2), 47–58.

Somashekar, B.R., 1983. A simple selectively integrated torsion-flexure coupled rapered beam element with transverse shear deformation. Computers and Structures 17 (3), 403–406.

Stoer, J., Bulirsch, R., 2002. Introduction to Numerical Analysis, second ed. Springer.

Takabatake, H., 1990. Cantilevered and linearly tapered thin-walled members. Journal of Structural Engineering ASCE 116 (4), 733–750.

Tang, X., 1993. Shape functions of tapered beam-column elements. Computers and Structures 4 (5), 943–953.

Tena-Colunga, A., 1996. Stiffness formulation for nonprismatic beam elements. Journal of Structural Engineering ASCE 122 (12), 1484–1489.

Thomas, J., Dokumaci, E., 1973. Improved finite elements for vibration analysis of tapered beams. Aeronautical Quarterly 24, 39–46.

To, C.W.S., 1979. Higher order tapered beam finite elements for vibration analysis. Journal of Sound and Vibration 63 (1), 33–50.

To, C.W.S., 1981. A linearly tapered beam finite element incorporating shear deformation and rotary inertia for vibration analysis. Journal of Sound and Vibration 78, 475–484.

Vu-Quoc, L., Léger, P., 1992. Efficient evaluation of the flexibility of tapered I-beams accounting for shear deformations. International Journal for Numerical Methods in Engineering 33, 553–566.

Wang, H.C., 1967. Generalized hypergeometric function solutions on the transverse vibration of a class of nonuniform beams. Journal of Applied Mechanics 34, 702–708.

Yang, Y., Chiou, H., 1987. Rigid body motion test for nonlinear analysis with beam elements. Journal of Engineering Mechanics ASCE 113 (9), 1404–1419.